JACS
JOURNAL OF THE AMERICAN CHEMICAL SOCIETY

Article

pubs.acs.org/JACS

# Locking Covalent Organic Frameworks with Hydrogen Bonds: General and Remarkable Effects on Crystalline Structure, Physical Properties, and Photochemical Activity

Xiong Chen,[†] Matthew Addicoat,[‡] Enquan Jin,[†] Lipeng Zhai,[†] Hong Xu,[†] Ning Huang,[†] Zhaoqi Guo,[†] Lili Liu,[‡] Stephan Irle,[‡] and Donglin Jiang*[,†]

[†]Department of Materials Molecular Science, Institute for Molecular Science, National Institutes of Natural Sciences, 5-1 Higashiyama, Myodaiji, Okazaki 444-8787, Japan

[‡]Department of Chemistry, Graduate School of Science, Nagoya University, Furo-cho, Chikusa-ku, Nagoya 464-8601, Japan

Supporting Information

**ABSTRACT:** A series of two-dimensional covalent organic frameworks (2D COFs) locked with intralayer hydrogen-bonding (H-bonding) interactions were synthesized. The H-bonding interaction sites were located on the edge units of the imine-linked tetragonal porphyrin COFs, and the contents of the H-bonding sites in the COFs were synthetically tuned using a three-component condensation system. The intralayer H-bonding interactions suppress the torsion of the edge units and lock the tetragonal sheets in a planar conformation. This planarization enhances the interlayer interactions and triggers extended $\pi$-cloud delocalization over the 2D sheets. Upon AA stacking, the resulting COFs with layered 2D sheets amplify these effects and strongly affect the physical properties of the material, including improving their crystallinity, enhancing their porosity, increasing their light-harvesting capability, reducing their band gap, and enhancing their photocatalytic activity toward the generation of singlet oxygen. These remarkable effects on the structure and properties of the material were observed for both freebase and metalloporphyin COFs. These results imply that exploration of supramolecular ensembles would open a new approach to the structural and functional design of COFs.

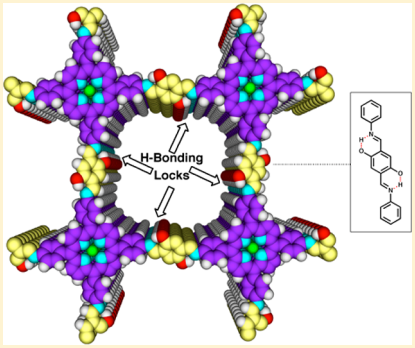


## INTRODUCTION

Covalent organic frameworks (COFs) are an attractive class of crystalline porous polymers that can integrate organic units with atomic precision into periodic structures.[1−8] Because of their structural regularity and discrete pore size, COFs serve as an intriguing design medium for gas adsorption and storage.[1−8] Among all COFs, two-dimensional (2D) COFs exhibit unique structures that feature 2D extended organic sheets and layered stacking structures, which generate periodic columnar $\pi$-arrays and ordered one-dimensional channels.[1−8] Recent progress has demonstrated that 2D COFs offer a novel platform for designing organic semiconductors with inherent intra- and intermolecular orderings.[2d,4,8] Notably, these structural features of 2D COFs are rarely achieved by other molecular, supramolecular, and polymeric materials.

Two key issues to be addressed include the development of the 2D sheet and its effect on the layered framework. Although the exploration of synthetic methods has greatly expanded the structural diversity of 2D COFs, in most cases, these critical issues are still unclear. This uncertainty is further complicated by the lack of single-crystal structures of 2D COFs. In this context, understanding of the structural evolution and functional origins of COFs is highly desirable. Recently, we have reported an interlayer strategy that involves introducing complementary force to the neighboring layers of electron-rich and deficient sheets, which control the stacking force of the resulting COFs and thus their properties.[4h] However, this strategy based on interlayer interactions does not provide valuable insights to the issues of sheet evolution and its effect on the structure and function of 2D COFs.

Here we report an intrasheet strategy that could elucidate the sheet evolution and its influence on the structure and functions of 2D COFs. For this purpose, a series of 2D porphyrin COFs with tunable content of intralayer hydrogen-bonding (H-bonding) interaction sites are synthesized using a three-component condensation system. Yaghi et al. have reported the nonfunctionalized imine-linked porphyrin COFs.[2f] Banerjee et al. have reported the mechanochemical synthesis of OH-functionalized COFs.[9] The H-bonding interactions suppress the torsion of the edge units and lock the tetragonal 2D sheets in a planar conformation. As a result, this planarization enhances the interlayer interactions and allows extended $\pi$ conjugation over the 2D sheets. Upon AA stacking, these interactions are further amplified to exert a positive influence on the physical properties of the material; the planar conformation of the 2D sheets leads to improved crystallinity, enhanced porosity, increased light-harvesting capability,

**Received:** May 8, 2014
**Published:** February 23, 2015





DOI: 10.1021/ja509602c
J. Am. Chem. Soc. 2015, 137, 3241−3247

**Chart 1. Schematic of the Synthesis of 2D Porphyrin COFs with Tunable Content of Hydrogen-Bonding Structures**

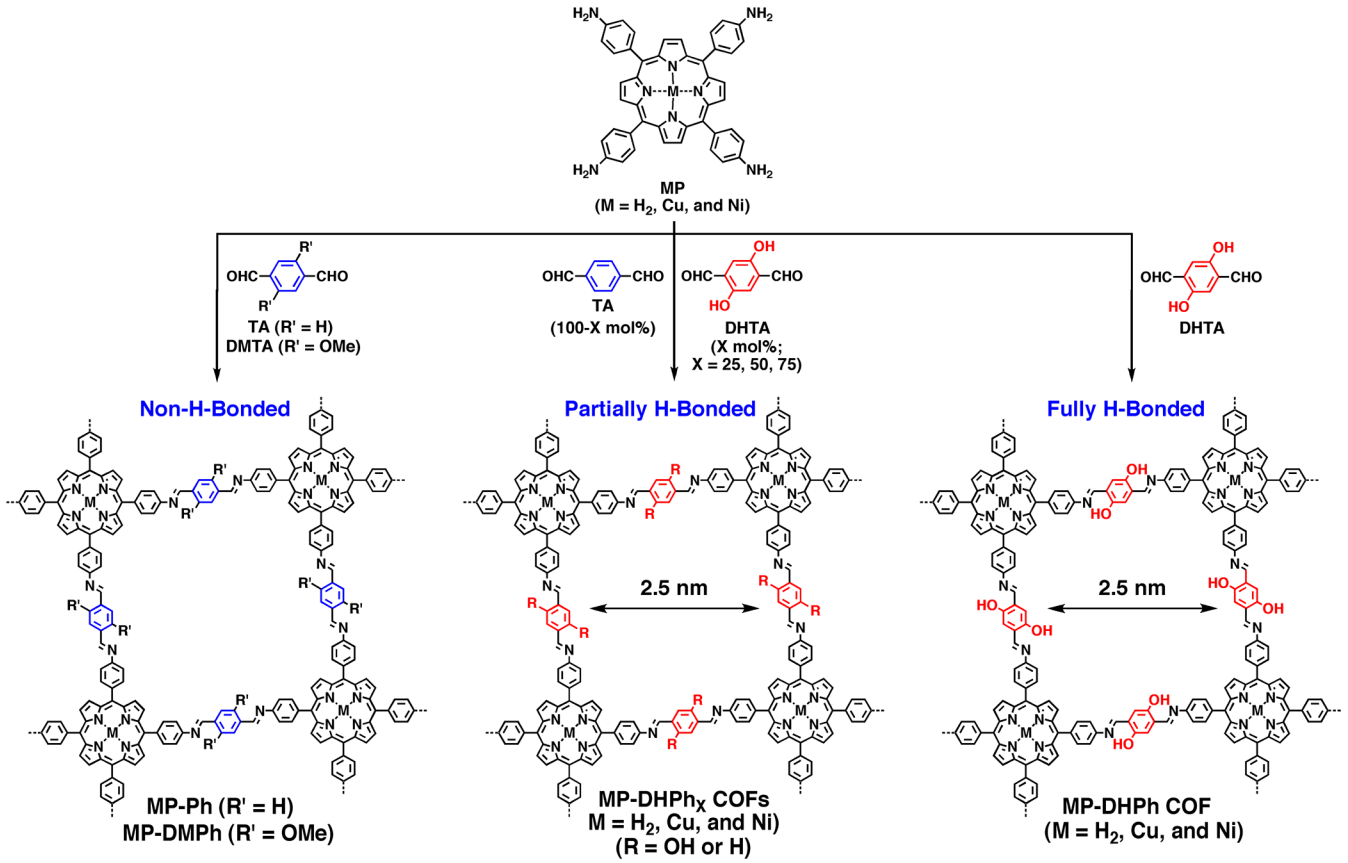


reduced band gap, and enhanced photocatalytic activity in the generation of singlet oxygen. These profound effects are observed for both freebase- and metalloporphyin COFs. The addition of supramolecular interactions to the COF architecture, together with its effect on the enhanced chemical stability reported previously,[9d] could be a key to elucidating the structural evolution and property origins of COFs.

## RESULTS AND DISCUSSION

**Synthesis and Characterization.** We demonstrated the intralayer supramolecular strategy by integrating H-bonding sites to the edge units of tetragonal 2D porphyrin COFs (Chart 1). We employed a mixture of dihydroxyterephthalaldehyde (DHTA) and terephthaladehyde (TA) at different molar ratios (X = [DHTA]/([TA] + [DHTA]) × 100) as a monomer to react with 5,10,15,20-tetrakis(4′-tetraphenylamino) porphyrin derivatives (MP; M = Cu, $H_2$, and Ni) for construction of 2D COFs, and the DHTA monomer forms H-bonding edges (Chart 1, X = 0: amorphous MP-Ph polymers, X = 25, 50, 75: MP-DHPh$_X$ COFs, X = 100: MP-DHPh COFs). Because acidic conditions may cause the protonation of pyrrole NH groups of free-base porphyrin and the demetalation of metalloporphyrins, we developed a new synthetic protocol that does not require acetic acid as a catalyst (Supporting Information (SI)). By screening the reaction conditions, including various different combinations of solvents, we observed that a mixture of *o*-dichlorobenzene and *n*-butanol under solvothermal conditions produces the MP-DHPh$_X$ COFs in 68−83% isolated yields (Table S1, Figure S1−S4). These reactions exhibited similar isolation yields, indicating that the reactivities of DHTA and TA are similar under solvothermal conditions. To confirm the TA:DHTA output in the COFs, we conducted elemental analysis of the MP-DHPh$_X$ COFs (X = 25, 50, 75, and 100); the results are summarized in Table S2. The results revealed that the oxygen content increased when the X value was increased, which is consistent with an increase in the concentration of OH groups at the edges of the MP-DHPh$_X$ COFs. To prove the structural homogeneity of the MP-DHPh$_X$ COFs (X = 25, 50, 75, and 100), we conducted field-emission scanning electron microscopy. As show in Figure S5, each MP-DHPh$_X$ COF assumes a homogeneous shape. These results rule out the possibility that the MP-DHPh$_X$ COFs comprised mixtures of crystalline COFs and amorphous polymers.

Infrared spectroscopy revealed that the C═N stretching band of the CuP-DHPh COF appeared at 1612 cm$^{-1}$ (Figure S2a, Table S3). The spectrum of a model compound bearing H-bonding interaction displayed a C═N band at 1612 cm$^{-1}$, and the H-bonding interaction has been identified by single crystal structure analysis.[10] By contrast, the C═N vibration band of the amorphous and nonporous CuP-Ph polymer without H-bonding interactions located at 1622 cm$^{-1}$. As the DHPh content increased, the C═N vibration band shifted from 1622 to 1616, 1613, and 1612 cm$^{-1}$ (Table S3). A similar trend in the shift of the C═N vibrational band was observed for the $H_2$P-DHPh$_X$ COFs and NiP-DHPh$_X$ COFs (Figure S2b,c, Tables S4, S5). These results indicate that the nitrogen atoms of C═N units form H-bonding interactions with the OH groups of DHPh units in the MP-DHPh$_X$ COFs (X = 25, 50, 75, and 100). Figure S3 displayed the thermogravimetric analysis of the COFs, which are stable up to 400 °C. Notably, the samples were predried overnight at 120 °C under a vacuum


DOI: 10.1021/ja509602c
J. Am. Chem. Soc. 2015, 137, 3241−3247

to remove any possible solvent molecules in the pores before the TGA measurements.

**Influence on Crystallinity.** The H-bonding interactions significantly effect on the crystallinity of the CuP-DHPh$_X$ COFs (Figure 1A and F). For example, the X-ray diffraction (XRD)

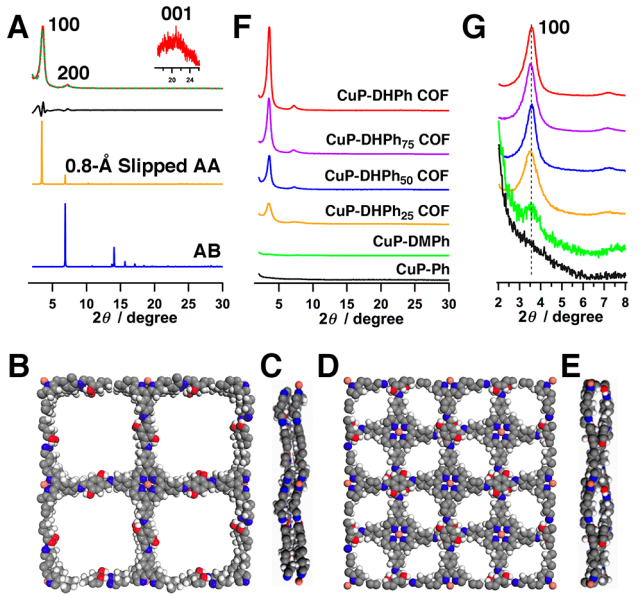


**Figure 1.** (A) Observed XRD pattern (red, inset: 001 facet) and profiles simulated using the Pawley refinement (green) and their difference (black), 0.8-Å slipped AA-stacking (orange), and staggered AB-stacking (blue) modes of the CuP-DHPh COF. (B, C) Unit-cell structure of 0.8-Å slipped AA-stacking mode. (D, E) Unit-cell structure of staggered AB-stacking mode. (F) XRD patterns of the CuP-DHPh$_X$ COFs and amorphous CuP-DMPh polymer. (G) Normalized 100 facets (the colors represent the same materials as in (F)).

pattern of the amorphous CuP-Ph polymer without H-bonding sites exhibited negligibly weak peaks compared to those in the CuP-DHPh$_X$ COFs (Figure 1F, black, Figure S1e). Changes in the reaction temperature and extension of reaction time did not improve the crystallinity of the amorphous polymers (Figure S1e). By contrast, the CuP-DHPh COF with H-bonding interactions was crystalline (red). A methoxy version of the polymer (Chart 1, amorphous CuP-DMPh polymer; Figure 1A, green; for characterizations, see SI), which is free of H-bonding interactions, was observed to be nearly amorphous. The amorphous nature of this MeO-functionalized polymer might be also caused by the steric hindrance of the bulky methoxy groups. The C═N vibration band in the spectrum of the amorphous CuP-DMPh polymer appeared at the same frequency (1616 cm$^{-1}$) as that in the spectrum of the methoxy version of the model compound free of H-bonding interactions (Figure S2d).

Interestingly, tuning of the DHPh content (content of H-bonding sites) caused a systematic change in the crystallinity, as revealed by the XRD profiles (Figure 1F). Notably, (a) these XRD curves were used strictly for a qualitative comparison and (b) best efforts were made to use same sample morphology, thickness, and other conditions. To clarify this point, the XRD patterns were normalized at the 100 facet (Figure 1G). The full-width half-maximum (fwhm) values of the 100 facet that best reflect the quality of the crystals were used for comparison. Indeed, the fwhm value decreased as the DHPh content was increased (Figure 1G). For example, the CuP-DHPh$_{25}$ COF (Figure 1G, orange curve) exhibited a large fwhm value of 0.74°, which decreased to 0.47°, 0.45°, and 0.42°, as the DHPh content increased to 50% (blue curve), 75% (purple curve), and 100% (red curve), respectively. The amorphous CuP-DMPh polymer (green curve) exhibited the largest fwhm value of 0.84°. Moreover, the amorphous CuP-Ph polymer (black curve) exhibited a 100 facet that was too broad for the fwhm estimation. These observations qualitatively suggest that an increase in the number of the H-bonding interaction sites results in greater COF crystallinity.

**Crystal-Structure Resolutions.** The XRD pattern of the CuP-DHPh COF exhibited peaks at 3.5°, 7.2°, and 22.9, which are assignable to the 100, 200, and 001 facets, respectively (Figure 1A, red). These XRD peaks indicate that the CuP-DHPh COF exhibites periodic ordering in all three dimensions. The Pawley refinement (green) using a unit cell of $\alpha = \beta = \gamma = 90°$, $a = b = 25.91$ Å, and $c = 3.79$ Å (Table S6) confirmed the peak assignment, as evidenced by their negligible difference (black). Interestingly, the $c$ parameter is smaller than that of the CuP-DHPh$_{50}$ COF ($c = 3.88$ Å), indicating that the H-bonding interactions maximize the layer interaction and minimize the unit-cell size. Crystal structural simulations (for coordinates, see SI) using the 0.8-Å slipped AA-stacking mode (Figure 1B and C) gave an XRD pattern (Figure 1A, orange) that reproduces the XRD peaks. By contrast, staggered AB-stacking offset by $a/2$ and $b/2$ gave an XRD pattern (blue) that did not reproduce the XRD peaks. In this case, the pores were overlapped by neighboring sheets (Figure 1D and E).

**Sheet Conformation and Stacking Modes.** The density-functional tight-binding (DFTB) method including Lennard–Jones (LJ) dispersion was used to elucidate the optimal sheet conformation of COFs. The optimized dihedral angle between the imine linkage and meso-phenyl units of porphyrin in the CuP-DHPh COF was 48°, whereas the total crystal stacking energy of the CuP-DHPh COF was 67.67 kcal mol$^{-1}$ per unit cell (Table S7). When the DHPh unit was replaced with a Ph group, this torsion angle increases to 64° and the total crystal stacking energy of the amorphous CuP-Ph polymer decreases to 60.88 kcal mol$^{-1}$ (Table S8). The amorphous CuP-DMPh polymer exhibited decreased planarity and required more energy to form crystalline frameworks (Table S9). Therefore, the H-bonding interactions triggered a more planar conformation, which endowed the COFs with strong $\pi$-stacking interactions and enhanced crystallinity.

**Generalization of the H-Bonding Effect: Crystallinity Issue.** Interestingly, the supramolecular effect was also observed for free-base porphyrin and other metalloporphyrin COFs (Chart 1). For example, the free-base H$_2$P-Ph without H-bonding sites on the edges is nearly amorphous (Figure 3A, black curve) and exhibited a low porosity, with a Brunauer–Emmett–Teller (BET) surface area of only 20 m$^2$ g$^{-1}$ (Figure 2E). Similarly, the crystallinity of H$_2$P-DHPh$_X$ COFs (Figure 3A) and NiP-DHPh$_X$ COFs (Figure 4A) increased as the concentration of H-bonding sites was increased, as indicated by decreased fwhm value of the 100 facets (Figure 3B, Figure 4B). The fwhm values were 0.88°, 0.42°, 0.38°, and 0.35° for H$_2$P-DHPh$_{25}$ COF (Figure 3B, orange), H$_2$P-DHPh$_{50}$ COF (blue), H$_2$P-DHPh$_{75}$ COF (purple), and H$_2$P-DHPh COF (red), respectively. The amorphous H$_2$P-Ph polymer did not show a distinct 100 facet that would allow the fwhm value to be determined (black curve). The fwhm value was 0.96°, 0.75°, 0.50°, 0.46°, and 0.43° for the NiP-Ph, NiP-DHPh$_{25}$ COF (Figure 4B, orange), NiP-DHPh$_{50}$ COF (blue), NiP-DHPh$_{75}$


DOI: 10.1021/ja509602c
J. Am. Chem. Soc. 2015, 137, 3241–3247

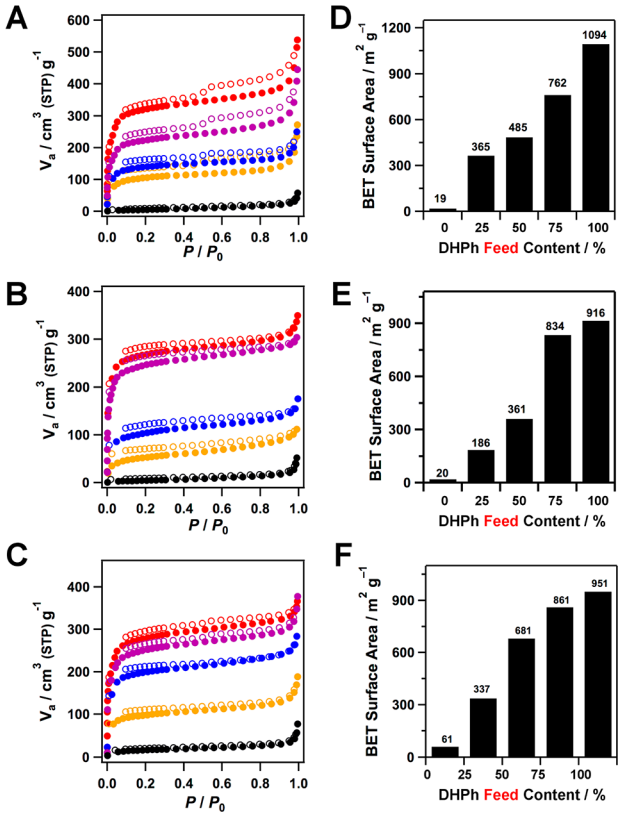


**Figure 2.** (A–C) Nitrogen sorption isotherms of (A) CuP-DHPh$_X$ COFs, (B) H$_2$P-DHPh$_X$ COFs, and (C) NiP-DHPh$_X$ COFs measured at 77 K (red: X = 100; purple: X = 75; blue: X = 50; orange: X = 25; black: X = 0; solid and open circles represent desorption and adsorption data, respectively). (D–F) The BET surface area of (D) CuP-DHPh$_X$ COFs, (E) H$_2$P-DHPh$_X$ COFs, and (F) NiP-DHPh$_X$ COFs.

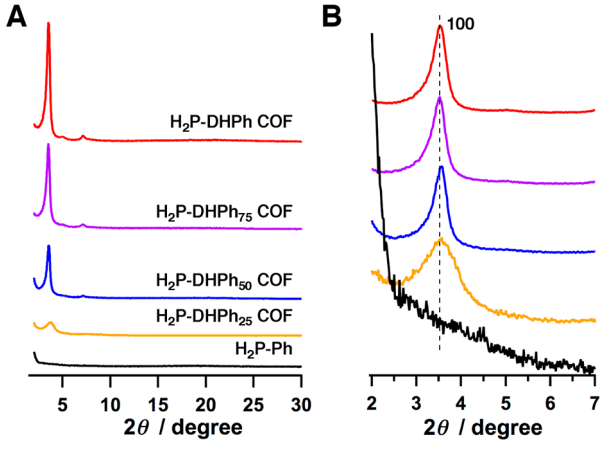


**Figure 3.** (A) XRD patterns of the H$_2$P-DHPh$_X$ COFs. (B) Normalized 100 facets of the H$_2$P-DHPh$_X$ COFs (the colors represent the same materials as in (A) and (B)).

COF (purple), and NiP-DHPh COF (red), respectively (Figure 4B). As a result of more planar structure of its NiP macrocycle, the NiP-Ph polymer without H-bonding sites was crystalline and exhibited clear XRD peaks (Figure 4B, black). Compared with the CuP-DHPh COF, the NiP-DHPh COF has a more planar sheet structure with a relatively small dihedral angle of 44° between the imine linkage and meso-phenyl units of porphyrin ring (Table S10).

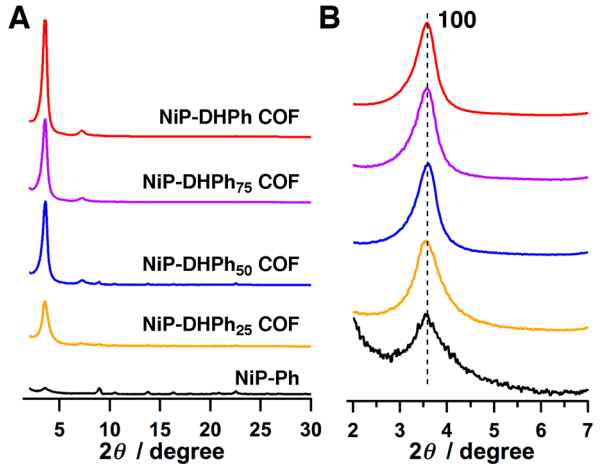


**Figure 4.** (A) XRD patterns of the NiP-DHPh$_X$ COFs. (B) Normalized 100 facets of the NiP-DHPh$_X$ (the colors represent the same materials as in (A) and (B)).

**Generalization of the H-Bonding Effect: Porosity Issue.** Remarkably, the H-bonding interactions led to enhanced porosity. For example, the amorphous CuP-Ph polymer (Figure 2A, black) is nonporous with a BET surface area of only 19 m$^2$ g$^{-1}$ (Figure 2D). The amorphous CuP-DMPh polymer has a BET surface area of 83 m$^2$ g$^{-1}$ (Table S11). The BET surface area increased drastically to 365, 485, 762, and 1094 m$^2$ g$^{-1}$ and the pore volume also increased steadily to 0.27, 0.30, 0.57, and 0.78 cm$^3$ g$^{-1}$, as the DHPh content was increased to 25, 50, 75, and 100%, respectively (Table S11). Pore distribution profiles revealed the existence of only one type of 2.5 nm-wide mesopore, which accounts for the porosity (Figure S6).

The H$_2$P-DHPh$_X$ COFs exhibited type IV nitrogen sorption curves (Figure 2B) and exhibited an increase in the BET surface area from 186 to 361, 834, and 916 m$^2$ g$^{-1}$, as the content of H-bonding sites was increased from 25 to 50, 75, and 100%, respectively (Figure 2E). The enhancement of the porosity by the H-bonding interaction was dependent on the enhanced crystallinity caused by the H-bonds. For example, the CuP-DHPh$_X$ COF series exhibited a much greater crystallinity enhancement compared with the H$_2$P-DHPh$_X$ COF series, which resulted in a better porosity improvement. The pore volume also increased from 0.16 to 0.26, 0.55, and 0.63 cm$^3$ g$^{-1}$ (Figure S7, Table S11). The BET surface area of the NiP-DHPh$_X$ COFs (Figure 2C) increased from 337 to 681, 861, and 951 m$^2$ g$^{-1}$ (Figure 2F) and the pore volume increased from 0.25 to 0.48, 0.63, and 0.69 cm$^3$ g$^{-1}$ (Figure S8, Table S11), as the content of H-bonding sites was increased from 25 to 50, 75, and 100%, respectively. Therefore, the H-bonding interactions enhance the porosity of the COFs.

**Generalization of the H-Bonding Effect: Influence on $\pi$-Conjugation.** The CuP-DHPh COF exhibited a broad Soret band centered at 494 nm, which was red-shifted by 51 and 33 nm from those of the CuP monomer and amorphous CuP-Ph polymer, respectively (Figure 5A). Similarly, the Soret band of the H$_2$P-DHPh COF was 505 nm, which was red-shifted by 53 and 25 nm from the H$_2$P monomer and amorphous H$_2$P-Ph polymer, respectively (Figure 5B). A more explicit change was observed for the NiP-DHPh COF, whose spectrum exhibited a continuous absorbance from 250 to 600 nm without a clear boundary between the Soret and Q-bands, indicating a more progressed $\pi$ electron delocalization (Figure 5C). These redshifts contrast the boronate-linked porphyrin COFs, which


DOI: 10.1021/ja509602c
J. Am. Chem. Soc. 2015, 137, 3241–3247

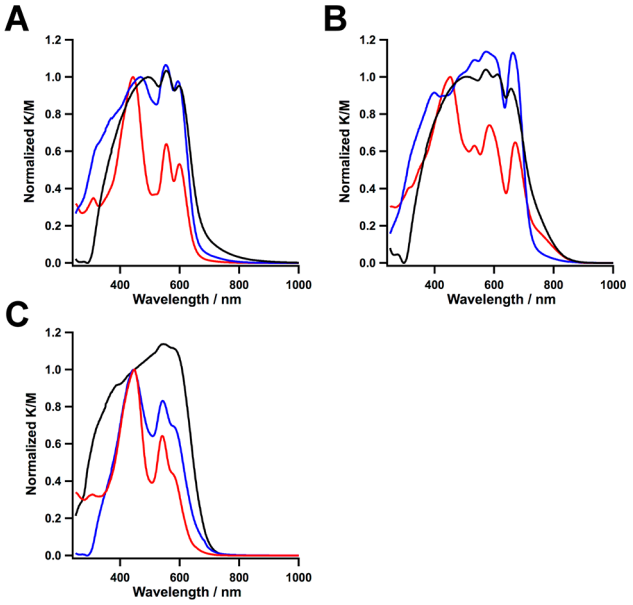


**Figure 5.** Electronic absorption spectral of (A) CuP-DHPh COF (black), CuP (red), amorphous CuP-Ph polymer (blue), (B) $H_2$P-DHPh COF (black), $H_2$P (red), amorphous $H_2$P-Ph polymer (blue), (C) NiP-DHPh COF (black), NiP (red), and NiP-Ph polymer (blue).

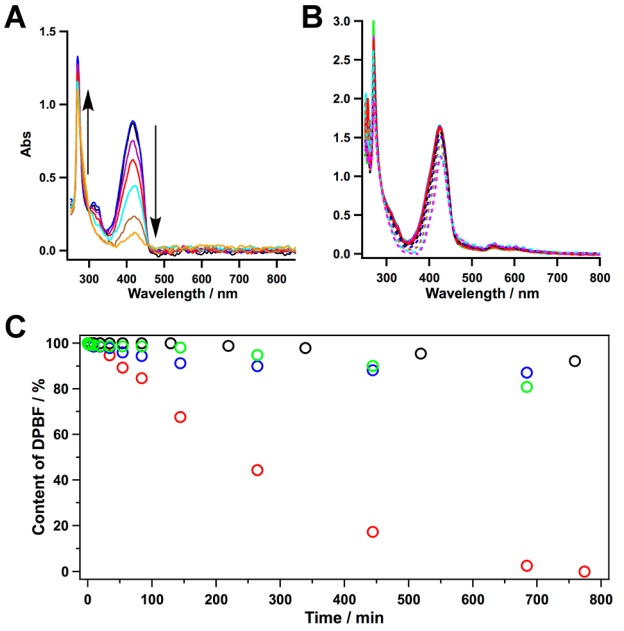


**Figure 6.** Absorption spectral changes of DPBF in the presence of (A) the CuP-DHPh COF and (B) the amorphous CuP-Ph polymer, in an oxygen-saturated DMF solution upon irradiation at 500 nm. (C) Effect of different photocatalysts (0.5 mg) on the reaction (black: monomeric CuTPP; blue: CuP-linear polymer; green: amorphous CuP-Ph polymer; red: CuP-DHPh COF).

do not exhibit a redshift in the Soret band because of their nonconjugated structure.[4d] The imine-linked tetragonal topology of the MP-DHPh COFs induces the $\pi$-conjugation.

**Generalization of the H-Bonding Effect: Influences on Light Harvesting and Bandgap.** Interestingly, the absorbance of the MP-DHPh COFs in the long-wavelength visible and near-infrared regions was greatly enhanced (Figure 5). For example, the relative intensity of the Q-band to the Soret band ($I_Q/I_{Soret}$) was 0.64 for the CuP monomer, which increased to 1.04 for the CuP-DHPh COF. Similarly, the $I_Q/I_{Soret}$ ratios for the $H_2$P-DHPh COF and NiP-DHPh COF were 1.04 and 1.14, respectively and the corresponding $I_Q/I_{Soret}$ ratios for their monomeric MPs are 0.74 and 0.64, respectively. These results indicate that the H-bonding interactions enhance the capability of light harvesting of visible photons. In comparison to the amorphous analogues, the H-bonded COFs exhibited redshifted absorption onset. As a result, the CuP-DHPh COF, $H_2$P-DHPh COF, and NiP-DHPh COF exhibited small band gaps of 1.36, 1.31, and 1.54 eV, respectively, which are smaller than those (1.40, 1.36, and 1.58 eV) of the amorphous MP-Ph polymers.

**Generalization of the H-Bonding Effect: Influence on Photochemical Activity.** The H-bonding interactions significantly affect the photocatalytic activity. We examined the photocatalytic activity of the COFs by using 1,3-diphenylisobenzofuran (DPBF) as a label for the singlet oxygen generation monitored by time-dependent electronic absorption spectroscopy (SI).[11] Indeed, the visible light irradiation of an oxygen-saturated DMF solution (2.3 mL) of DPBF (50 $\mu$M) in the presence of the CuP-DHPh COF (0.5 mg) triggered a steady conversion of molecular oxygen into singlet oxygen, as evidenced by the spectral change of DPBF, with clear isosbestic points (Figure 6A).

We utilized three CuP derivatives, including the monomeric CuTPP (copper tetrakisphenyl porphyrin), the amorphous CuP-Ph polymer without H-bonding sites, and the linear CuP polymer, as controls for the molecular oxygen activation (Figure S9). As a result, the monomeric CuTPP exhibited only very small spectral changes (Figure S9a), with a conversion of less than 5% (Figure 6C, black circles); these results indicate that the monomeric CuTPP system is less active. In the case of the linear CuP polymer (Figure S9b), the spectral changes were also very small. The time-dependent profile revealed that the reaction catalyzed by the CuP-linear polymer was quite sluggish, with a conversion of only 8% (Figure 6C, blue dots). Moreover, the amorphous CuP-Ph polymer without H-bonding sites on the edges exhibited a similar low rate of reaction (Figure 6B; Figure 6C, green circles). As evidenced in Figure 6C, the CuP-DHPh COF is exceptionally active as a photocatalyst, exhibiting a 10−20-fold enhancement in activity compared with those of other CuP derivatives.

**Mechanistic Insights into the Photocatalytic Activity.** To elucidate which wavelength of visible light is most effective, we used 500, 550, and 600 nm light for the photocatalytic reaction in the presence of CuP-DHPh COF (Figure S9). Figure 7A summarizes these results. Although all these three wavelengths triggered the photocatalytic reaction, the visible light with wavelengths of 500 (red circles) and 550 nm (blue circles) was superior to that with a wavelength of 600 nm (black circles). This result was caused by the weaker absorption of the COF and the weaker power of the light source at 600 nm. If normalized, the photocatalytic activities of these three wavelengths of light are similar to each other. These results indicate that the COF can harvest a wide range of visible photons for driving chemical transformation.

Furthermore, we examined the performance of the NiP-DHPh COF and the $H_2$P-DHPh COF in photocatalytic singlet oxygen evolution (Figure 7B). Surprisingly, the conversion of DPBF in the presence of the $H_2$P-DHPh COF was complete in a much shorter time, indicating that the $H_2$P-DHPh COF (red circles) exhibits enhanced photocatalytic activity compared with


DOI: 10.1021/ja509602c
J. Am. Chem. Soc. 2015, 137, 3241−3247

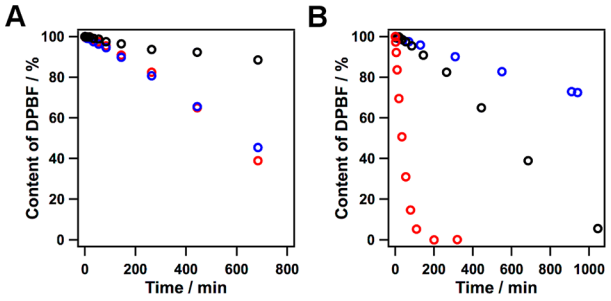


**Figure 7.** (A) Effect of light wavelength (red: 500 nm; blue: 550 nm; black: 600 nm) on the reaction in the presence of the CuP-DHPH COF (0.1 mg). (B) Effect of different COFs (0.1 mg) on the reaction (black: CuP-DHPh COF; blue: NiP-DHPh COF; red: $H_2$P-DHPh COF).

the CuP-DHPh COF (black circles) and the NiP-DHPh COF (blue circles). We conducted the photocatalytic reactions using all the members of COFs with different content of H-bonding sites (Figure S10). Figure 8 summarized the results. For each series of COFs, the photocatalytic activity of the COFs increased as the content of H-bonding site was increased.

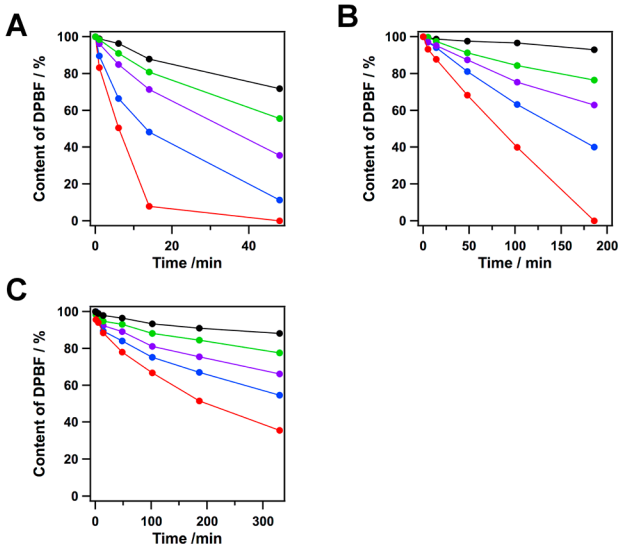


**Figure 8.** Effect of the content of H-bonding site on the photocatalytic activity of (A) $H_2$P-DHPh$_X$ COFs, (B) CuP-DHPh$_X$ COFs, and (C) NiP-DHPh$_X$ COFs (black: X = 0; green: X = 25; purple: X = 50; blue: X = 75; red: X = 100).

To clarify the activity gap between the $H_2$P-DHPh COF and the CuP-DHPh COF, we measured time-resolved fluorescence decay spectra of the singlet oxygen by monitoring the fluorescence at 1270 nm.[12] The $H_2$P-DHPh COF and CuP-DHPh COF were dispersed in an oxygen-saturated ether/ethanol/toluene mixture solution (2/1/1 by vol.) and subjected to time-resolved fluorescence spectroscopic measurements at 77 K (Figure 9). The average lifetime of singlet oxygen in the case of the CuP-DHPh COF was evaluated to be as long as 29.43 ns (Figure 9A). In sharp contrast, in the presence of the $H_2$P-DHPh COF, the lifetime of singlet oxygen was only 1.23 ns (Figure 9B). Because the oxidation of DPBF by the electrophilic singlet oxygen is accompanied by electron transfer, a short lifetime of singlet oxygen indicates a facilitated electron

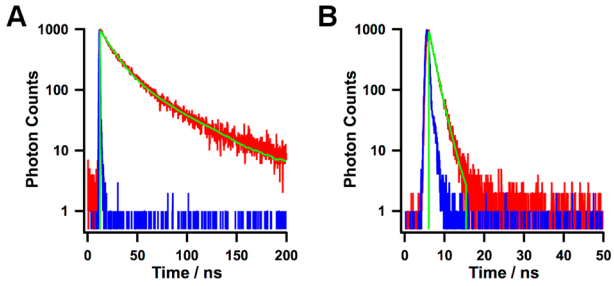


**Figure 9.** Fluorescence decay profile of singlet oxygen in the presence of (A) the CuP-DHPh COF and (B) the $H_2$P-DHPh COF in ether/ethanol/toluene (2/1/1 by vol.) under liquid $N_2$ at 77 K ($\lambda_{ex}$ = 532 nm, $\lambda_{em}$ = 1270 nm). The blue curve is the instrument response function (IRF) profile.

transfer process; therefore, the conversion of DPBF by the $H_2$P-DHPh COF was more efficient.

The transformation of molecular oxygen to singlet oxygen is triggered by the triplet state of a photocatalyst. Accordingly, the MP-DHPh COF can efficiently generate the triplet state for the activation of molecular oxygen. The large difference between the crystalline MP-DHPh COF and the other amorphous analogues indicates that the COF architecture is powerful for controlling photoinduced excited states and for facilitating the generation of the triplet state. Although conventional porphyrin derivatives are not efficient photocatalysts, metalloporphyrins with noble-metal species, such as platinum or palladium, have been extensively utilized for the activation of molecular oxygen because of their highly efficient generation of the triplet state. In this sense, the MP-DHPh COF without noble metal offers a new approach to this fundamental yet challenging photocatalytic reaction.

## CONCLUSIONS

In summary, we have shed new light on the supramolecular interactions of COFs and their effects on the structural evolution of 2D sheets and layered frameworks. This investigation was made possible by the development of a three-component condensation system that allowed the H-bonding interactions for a series of prophyrin COFs to be tuned in a predesigned and systematical manner. This approach enabled us to gain insights into the remarkable effects of these interactions on the structure, physical properties, and photochemical functions of the resulting COFs, including their crystallinity, porosity, $\pi$-cloud delocalization, light-harvesting ability, band gap, photocatalytic activity, and ability to generate singlet oxygen. The results of this work also suggest that the COF architecture allows for the integration of supramolecular docking sites with precisely designed positions and contents. Thus, the exploration of supramolecular ensembles will reveal new chemical features of COFs. For example, in addition to H-bonding interactions, the integration of other interactions, such as metal ligation, hydrophobic interactions, $\pi-\pi$ interactions, and van der Waals interactions, will provide new opportunities for the emerging field of COFs.

## ASSOCIATED CONTENT

### Supporting Information

Synthetic details, methods, spectral profiles, microscopic images, computational results, and atomistic coordinates and atomic net charges. This material is available free of charge via the Internet at http://pubs.acs.org.



DOI: 10.1021/ja509602c
J. Am. Chem. Soc. 2015, 137, 3241−3247

## AUTHOR INFORMATION


### Corresponding Author

jiang@ims.ac.jp


### Notes

The authors declare no competing financial interest.

## ACKNOWLEDGMENTS

This work was supported by a Grant-in-Aid for Scientific Research (A) (24245030) from MEXT (Ministry of Education, Culture, Sports, Science and Technology, Japan). We thank Hamamatsh Photonics for the time-resolved fluorescence spectroscopies measurement of singlet oxygen.

## REFERENCES


(1) Feng, X.; Ding, X.; Jiang, D. *Chem. Soc. Rev.* **2012**, *41*, 6010.

(2) (a) Côté, A. P.; Benin, A. I.; Ockwig, N. W.; O'Keeffe, M.; Matzger, A. J.; Yaghi, O. M. *Science* **2005**, *310*, 1166. (b) Côté, A. P.; El-Kaderi, H. M.; Furukawa, H.; Hunt, J. R.; Yaghi, O. M. *J. Am. Chem. Soc.* **2007**, *129*, 12914. (c) El-Kaderi, H. M.; Hunt, J. R.; Mendoza-Cortés, J. L.; Côté, A. P.; Taylor, R. E.; O'Keeffe, M.; Yaghi, O. M. *Science* **2007**, *316*, 268. (d) Hunt, J. R.; Doonan, C. J.; LeVangie, J.D.; Côté, A. P.; Yaghi, O. M. *J. Am. Chem. Soc.* **2008**, *130*, 11872. (e) Doonan, C. J.; Tranchemontagne, D. J.; Glover, T. G.; Hunt, J. H.; Yaghi, O. M. *Nat. Chem.* **2010**, *2*, 235. (f) Wan, S.; Gandara, F.; Asano, A.; Furukawa, H.; Saeki, A.; Dey, S. K.; Liao, L.; Ambrogio, M. W.; Botros, Y. Y.; Duan, X.; Seki, S.; Stoddart, J. F.; Yaghi, O. M. *Chem. Mater.* **2011**, *23*, 4094. (g) Uribe-Romo, F. J.; Doonan, C. J.; Furukawa, H.; Oisaki, K.; Yaghi, O. M. *J. Am. Chem. Soc.* **2011**, *133*, 11478. (h) Zhang, Y.; Su, J.; Furukawa, H.; Yun, Y.; Gándara, F.; Duong, A.; Zou, X.; Yaghi, O. M. *J. Am. Chem. Soc.* **2013**, *135*, 16336.

(3) (a) Tilford, R. W.; Gemmill, W. R.; zur Loye, H. C.; Lavigne, J. J. *Chem. Mater.* **2006**, *18*, 5296. (b) Tilford, R. W.; Mugavero, S. J., III; Pellechia, P. J.; Lavigne, J. J. *Adv. Mater.* **2008**, *20*, 2741. (c) Lanni, L. M.; Tilford, R. W.; Bharathy, M.; Lavigne, J. J. *J. Am. Chem. Soc.* **2011**, *133*, 13975.

(4) (a) Wan, S.; Guo, J.; Kim, J.; Ihee, H.; Jiang, D. *Angew. Chem., Int. Ed.* **2008**, *47*, 8826. (b) Wan, S.; Guo, J.; Kim, J.; Ihee, H.; Jiang, D. *Angew. Chem., Int. Ed.* **2009**, *48*, 5439. (c) Ding, X.; Guo, J.; Feng, X.; Honsho, Y.; Guo, J.; Seki, S.; Maitarad, P.; Saeki, A.; Nagase, S.; Jiang, D. *Angew. Chem., Int. Ed.* **2011**, *50*, 1289. (d) Nagai, A.; Guo, Z.; Feng, X.; Jin, S.; Chen, X.; Ding, X.; Jiang, D. *Nat. Commun.* **2011**, *2*, 536 DOI: 10.1038/ncomms1542. (e) Ding, X.; Chen, L.; Honsho, Y.; Feng, X.; Saengsawang, O.; Guo, J.; Saeki, A.; Seki, S.; Irle, S.; Nagase, S.; Vudhichai, P.; Jiang, D. *J. Am. Chem. Soc.* **2011**, *133*, 14510. (f) Feng, X.; Liu, L.; Honsho, Y.; Saeki, A.; Seki, S.; Irle, S.; Dong, Y.; Nagai, A.; Jiang, D. *Angew. Chem., Int. Ed.* **2012**, *51*, 2618. (g) Feng, X.; Chen, L.; Honsho, Y.; Sa Saengsawang, O.; Liu, L.; Wang, L.; Saeki, A.; Irle, S.; Seki, S.; Dong, Y.; Jiang, D. *Adv. Mater.* **2012**, *24*, 3026. (h) Chen, X.; Addicoat, M.; Irle, S.; Nagai, A.; Jiang, D. *J. Am. Chem. Soc.* **2013**, *135*, 546. (i) Jin, S.; Ding, X.; Feng, X.; Supur, M.; Furukawa, K.; Takahashi, S.; Addicoat, M.; El-Khouly, M.; Nakamura, T.; Irle, S.; Fukuzumi, S.; Nagai, A.; Jiang, D. *Angew. Chem., Int. Ed.* **2013**, *52*, 2017. (j) Nagai, A.; Chen, X.; Feng, X.; Ding, X.; Guo, Z.; Jiang, D. *Angew. Chem., Int. Ed.* **2013**, *52*, 3770. (k) Jin, S.; Furukawa, K.; Addicoat, M.; Chen, L.; Takahashi, S.; Irle, S.; Nakamura, T.; Jiang, D. *Chem. Sci.* **2013**, *4*, 4505. (l) Dalapati, S.; Jin, S.; Gao, J.; Xu, Y.; Nagai, A.; Jiang, D. *J. Am. Chem. Soc.* **2013**, *135*, 17310. (m) Guo, J.; Xu, Y.; Jin, S.; Chen, L.; Kaji, T.; Honsho, Y.; Addicoat, M.; Kim, J.; Saeki, A.; Ihee, H.; Seki, S.; Irle, S.; Hiramoto, M.; Gao, J.; Jiang, D. *Nat. Commun.* **2013**, *4*, 2736 DOI: 10.1038/ncomms3736. (n) Xu, H.; Chen, X.; Gao, J.; Lin, J.; Addicoat, M.; Irle, S.; Jiang, D. *Chem. Commun.* **2014**, *47*, 1292. (o) Chen, X.; Huang, N.; Gao, J.; Xu, H.; Xu, F.; Jiang, D. *Chem. Commun.* **2014**, *50*, 6161. (p) Jin, S.; Sakurai, T.; Kowalczyk, T.; Dalapati, S.; Xu, F.; Wei, H.; Chen, X.; Gao, J.; Seki, S.; Irle, S.; Jiang, D. *Chem.—Eur. J.* **2014**, *20*, 14608.

(5) (a) Spitler, E. L.; Dichtel, W. R. *Nat. Chem.* **2010**, *2*, 672. (b) Colson, J. W.; Woll, A. R.; Mukherjee, A.; Levendorf, M. P.; Spitler, E. L.; Shields, V. B.; Spencer, M. G.; Park, J.; Dichtel, W. R. *Science* **2011**, *332*, 228. (c) Spitler, E. L.; Giovino, M. R.; White, S. L.; Dichtel, W. R. *Chem. Sci.* **2011**, *2*, 1588. (d) Spitler, E. L.; Koo, B. T.; Novotney, J. L.; Colson, J. W.; Uribe-Romo, F. J.; Gutierrez, G. D.; Clancy, P.; Dichtel, W. R. *J. Am. Chem. Soc.* **2011**, *133*, 19416. (e) Bunck, D. N.; Dichtel, W. R. *Angew. Chem., Int. Ed.* **2012**, *51*, 1885. (f) Spitler, E. L.; Colson, J. W.; Uribe- Romo, F. J.; Woll, A. R.; Giovino, M. R.; Saldivar, A.; Dichtel, W. R. *Angew. Chem., Int. Ed.* **2012**, *51*, 2623. (g) Bunck, D. N.; Dichtel, W. R. *Chem. Commun.* **2013**, *49*, 2457. (h) DeBlase, C. R.; Silberstein, K. E.; Truong, T.-T.; Abruña, H. D.; Dichtel, W. R. *J. Am. Chem. Soc.* **2013**, *135*, 16821. (i) Bunck, D. N.; Dichtel, W. R. *J. Am. Chem. Soc.* **2013**, *135*, 14952.

(6) (a) Campbell, N. L.; Clowes, R.; Ritchie, L. K.; Cooper, A. I. *Chem. Mater.* **2009**, *21*, 204. (b) Ren, S.; Bojdys, M. J.; Dawson, R.; Laybourn, A.; Khimyak, Y. Z.; Adams, D. J.; Cooper, A. I. *Adv. Mater.* **2012**, *24*, 2357.

(7) (a) Kuhn, P.; Antonietti, M.; Thomas, A. *Angew. Chem., Int. Ed.* **2008**, *47*, 3450. (b) Bojdys, M. J.; Jeromenok, J.; Thomas, A.; Antonietti, M. *Adv. Mater.* **2010**, *22*, 2202.

(8) (a) Patwardhan, S. A. A.; Kocherzhenko, F.; Grozema, C.; Siebbeles, L. D. A. *J. Phys. Chem. C* **2011**, *115*, 11768. (b) Dogru, M.; Handloser, M.; Auras, F.; Kunz, T.; Medina, D.; Hartschuh, A.; Knochei, P.; Bein, T. *Angew. Chem., Int. Ed.* **2013**, *52*, 2920. (c) Ding, S. Y.; Gao, J.; Wang, Q.; Zhang, Y.; Song, W.; Su, C.; Wang, W. *J. Am. Chem. Soc.* **2011**, *133*, 19816. (d) Rabbani, M. G.; Sekizkardes, A. K.; Kahveci, Z.; Reich, T. E.; Ding, R.; El-Kaderi, H. M. *Chem.—Eur. J.* **2013**, *19*, 3324. (e) Berlanga, I.; Mas-Ballesté, R.; Zamora, F. *Chem. Commun.* **2012**, *48*, 7976. (f) Bertrand, G. H. V.; Michaelis, V. K.; Ong, T.; Griffin, R. G.; Dincă, M. *Proc. Natl. Acad. Sci. U. S. A.* **2013**, *110*, 4923. (g) Beaudoin, D.; Maris, T.; Wuest, J. D. *Nat. Chem.* **2013**, *5*, 830. (h) Stegbauer, L.; Schwinghammer, K.; Lotsch, B. V. *Chem. Sci.* **2014**, *5*, 2789. (i) Medina, D. D.; Werner, V.; Auras, F.; Tautz, R.; Dogru, M.; Schuster, J.; Linke, S.; Döblinger, M.; Feldmann, J.; Knochel, P.; Bein, T. *ACS Nano* **2014**, *8*, 4042. (j) Guan, C.-Z.; Wang, D.; Wan, L.-J. *Chem. Commun.* **2012**, *48*, 2943. (k) Liu, X.-H.; Guan, C.-Z.; Ding, S.-Y.; Wang, W.; Yan, H.-J.; Wang, D.; Wan, L.-J. *J. Am. Chem. Soc.* **2013**, *135*, 10470. (l) Liu, X.-H.; Guan, C.-Z.; Wang, D.; Wan, L.-J. *Adv. Mater.* **2014**, *26*, 6912. (m) Fang, Q.; Zhuang, Z.; Gu, S.; Kaspar, R. B.; Zheng, J.; Wang, J.; Qiu, S.; Yan, Y. *Nat. Commun.* **2014**, *5*, 4503 DOI: 10.1038/ncomms5503.

(9) (a) Kandambeth, S.; Malick, A.; Lukose, B.; Mane, M. V.; Hein, T.; Banerjee, R. *J. Am. Chem. Soc.* **2012**, *134*, 19524. (b) Biswal, B. P.; Chandra, S.; Kandambeth, S.; Lukose, B.; Heine, T.; Banerjee, R. *J. Am. Chem. Soc.* **2013**, *135*, 5328. (c) Chandra, S.; Kandambeth, S.; Biswal, B. P.; Lukose, B.; Kunjir, S. M.; Chaudhary, M.; Babarao, R.; Heine, T.; Banerjee, R. *J. Am. Chem. Soc.* **2013**, *135*, 17853. (d) Kandambeth, S.; Shinde, D. B.; Panda, M. K.; Lukose, B.; Heine, T.; Banerjee, R. *Angew. Chem., Int. Ed.* **2013**, *52*, 13052. (e) Chandra, S.; Kundu, T.; Kandambeth, S.; BabaRao, R.; Marathe, Y.; Kunjir, S. M.; Banerjee, R. *J. Am. Chem. Soc.* **2014**, *136*, 6570.

(10) Inabe, T.; Hoshino, N.; Mitani, T.; Maruyama, Y. *Bull. Chem. Soc. Jpn.* **1989**, *62*, 2245.

(11) Wolfgang, S.; Holger, K.; Dieter, W.; Steffen, H.; Beate, R.; Gunter, S. *J. Porphyrins Phthalocyanines* **1998**, *2*, 145.

(12) DeRosa, M. C.; Crutchley, R. J. *Coord. Chem. Rev.* **2002**, *233–234*, 351.




DOI: 10.1021/ja509602c
*J. Am. Chem. Soc.* 2015, 137, 3241−3247